Thermoelectric power factor of composites

A. Riss⬤,[1,*] F. Garmroudi⬤,[1] M. Parzer⬤,[1] A. Pustogow⬤,[1] T. Mori⬤,[2,3] and E. Bauer[1]

[1]*Institute of Solid State Physics, Technische Universität Wien, Vienna 1040, Austria*

[2]*International Center for Materials Nanoarchitectonics (WPI-MANA), National Institute for Materials Science,*
Tsukuba 305-0044, Japan

[3]*Graduate School of Pure and Applied Science, University of Tsukuba, Tsukuba 305-8577, Japan*

To improve the performance of thermoelectric materials, a highly effective and widely implemented approach is to create multiphase composites. These composites are designed to impede phononic heat transport, which accounts for the majority of thermal conductivity in conventional thermoelectric semiconductors. In 1999, Bergman and Fel [J. Appl. Phys. 85(12), 8205–8216 (1999)] reported that also the electronic properties, specifically the power factor $S^2\sigma$, can be significantly enhanced in two-phase composites consisting of a highly conducting, simple metal and a high-performance thermoelectric arranged in an optimal manner, sparking great experimental interest. In this work, we challenge the theoretical results of Bergman and Fel and the conclusions drawn therein by utilizing a simple serial model. We show that, while the improvement of the power factor is indeed extraordinary, the results lead to a misleading interpretation of the overall thermoelectric performance of the material. As a result, we argue that the power factor is not a suitable metric for evaluating multiphase materials and composites, and that the figure of merit zT must be used instead. Nonetheless, we demonstrate that the best thermoelectric composite consists of a highly conductive metal and a high-performance thermoelectric.

I. INTRODUCTION

In times of rising energy consumption, there is an increasing demand to use energy more efficiently. One promising solution are thermoelectric materials, which can convert waste heat to electrical energy by making use of the Seebeck effect. The efficiency of such a material is determined by the dimensionless figure of merit $zT = (S^2\sigma/\lambda)T$, which is composed of the Seebeck coefficient S, the electrical conductivity σ, and the thermal conductivity λ. Single-phase bulk compounds have been intensively studied over the past decades, resulting in very efficient state-of-the-art materials such as Bi_2Te_3 [1,2], Pb-Te [3–5], Si-Ge [6,7], Sn-Se [8–10], skutterudites [11–13], or half-Heusler alloys [14–16] with large figures of merit.

Driven by the requirement to decouple thermal and electrical transport in thermoelectric materials, more sophisticated strategies have been employed, such as the synthesis of nanowires [17,18], thin films [19,20], as well as nanostructured materials and multiphase composites [21–24]. For composites comprising different materials or structures, effects like a reduction of the lattice thermal conductivity from increased phonon scattering at defects

on various length scales [25–27] and an increase of the Seebeck coefficient due to energy filtering at boundaries [26,28–30] can significantly increase the thermoelectric performance. However, for these multiphase materials, a more fundamental question arises: How and to what extent do the thermoelectric properties of the individual constituents contribute toward the overall properties of the composite?

In the 1990s, Bergman *et al.* claimed in two studies that a "high-performance thermoelectric" and a "benign metal," i.e., a metal with high electrical and thermal conductivity, combined in a favourable spatial configuration, can drastically boost the power factor (PF) $\mathcal{P} = S^2\sigma$ [31] but not the figure of merit zT [32]. In the absence of intrinsic property changes, such as interface effects, this would restrict the potential of composites to a high PF. Numerous studies have supported the occurrence of a largely enhanced power factor either theoretically or experimentally [33–41]. On the other hand, a debate about the merit of a boosted power factor due to incorporation of a simple metal is still missing.

Here, we inspect the relevant physical processes in composites and elucidate, based on a simple model, why the power factor is seemingly enhanced in such a system, in accord with the calculations by Bergman and Fel [31]. The model largely disregards the influences of interfaces on

*alexander.riss@tuwien.ac.at

electrical and thermal transport, which are usually present in composites and modify the measured properties. Nevertheless, our results demonstrate that the power factor is misinterpreted in these cases and overestimates the performance of such composite materials. Ultimately, we show in a straightforward manner that PF is an ill-defined quantity and performance indicator for the real power output of a material consisting of at least two phases. This will shine a new light on the research on composites and raise awareness of the ambivalent properties. Lastly, we highlight that, against common intuition, a two-phase heterostructure consisting of a thermoelectric with high zT and a perfect metal with high electrical and thermal conductivity is nonetheless the optimal thermoelectric composite.

II. THERMOELECTRIC PROPERTIES OF A SERIAL THERMOELECTRIC-METAL COMPOSITE

Bergman and Fel calculated the overall thermoelectric properties of thermoelectric-metal composites for several different spatial configurations [31]. They reported that the power factor can be improved through either alternating serial slabs or a spherical structure where the metal is coated by the thermoelectric material. The latter is often a good approximation to more realistic structures, as stated by the authors. In the present study, we will focus on the slab configuration, since it is easier to model and provides a better understanding about the origin of the apparent performance changes. Nonetheless, the qualitative similarity between the two configurations [31] allows our results to be extended to composites in general.

Figure 1(a) shows the model with the respective quantities of the thermoelectric and the metal used to calculate the overall properties. It is similar to the one used by Bergman and Fel, but with only one interface instead of alternating slabs. When ignoring interface effects, as done in both studies, these two models are equivalent. Figure 1(b) provides a realistic example for the application of the model in a two-phase composite material.

A. Power factor

For a better understanding, we will first calculate the total power factor of a serial connection of a thermoelectric material with large S and an ideal metal with $\rho_{\text{me}} \to 0$; therefore, $\lambda_{\text{me}} \to \infty$ due to the Wiedemann-Franz law. In the following, the total thermoelectric properties of the composite are written without index. From $\lambda_{\text{me}} \to \infty$ of the metal, it follows that the temperature at the interface $T_I = T_C$, and the whole temperature drop occurs in the thermoelectric material, yielding the thermovoltage

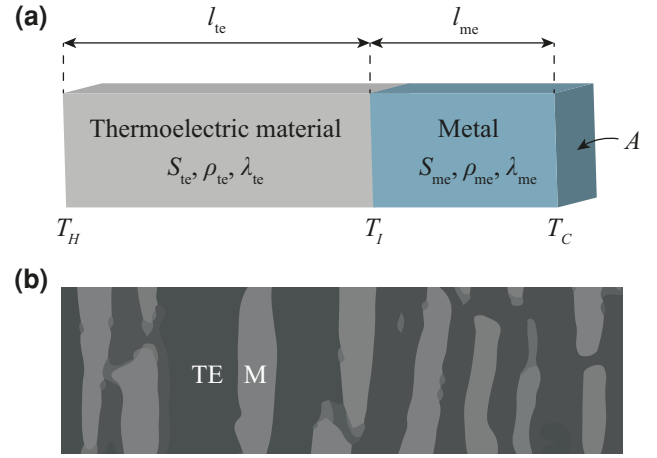$$U = S_{\text{te}}(T_H - T_C) = S_{\text{te}}\Delta T. \tag{1}$$

FIG. 1. (a) Schematic sketch of a serial connection of a thermoelectric material with length l_{te} and a metal with length l_{me}. Both materials have individual Seebeck coefficients S, electrical resistivities ρ, and thermal conductivities λ. The hot temperature at the end of the thermoelectric material, the temperature at the interface, and the cold temperature at the end of the metal are denoted as T_H, T_I, and T_C, respectively. (b) Sketch of the microstructure for a fictitious thermoelectric-metal (TE-M) composite material with a serial slab configuration.

The total Seebeck coefficient S is calculated as $S = U/\Delta T$, thus

$$S = S_{\text{te}}. \tag{2}$$

The total resistance only comprises ρ_{te} due to $\rho_{\text{me}} = 0$ in the ideal metal, which gives

$$\rho = R_{\text{te}}\frac{A}{l_{\text{te}} + l_{\text{me}}} = \rho_{\text{te}}\frac{l_{\text{te}}}{l_{\text{te}} + l_{\text{me}}} = \rho_{\text{te}}\delta_{\text{te}}, \tag{3}$$

with the volume fraction of the thermoelectric material δ_{te}. While the Seebeck coefficient is not affected by the metal, the resistivity—obtained by averaging the total resistance over the volume of the entire composite—seemingly decreases due to $\delta_{\text{te}} < 1$, resulting in an increase of the total power factor:

$$\mathcal{P} = \frac{S^2}{\rho} = \frac{S_{\text{te}}^2}{\rho_{\text{te}}\delta_{\text{te}}} = \mathcal{P}_{\text{te}}\frac{1}{\delta_{\text{te}}}. \tag{4}$$

Before discussing the physical meaning of Eq. (4), let us examine a more realistic scenario with finite resistivity and Seebeck coefficient ($S_{\text{me}} \ll S_{\text{te}}$) in the metal. The temperature differences across the thermoelectric material and the metal, $\Delta T_{\text{te}} = T_H - T_I$ and $\Delta T_{\text{me}} = T_I - T_{\text{me}}$, can be calculated from the thermal conductance $C_i = \lambda_i A/l_i$ of both

materials:

$$\Delta T_{\text{te}} = \frac{C_{\text{me}}}{C_{\text{te}} + C_{\text{me}}} \Delta T = \frac{l_{\text{te}}\lambda_{\text{me}}}{l_{\text{me}}\lambda_{\text{te}} + l_{\text{te}}\lambda_{\text{me}}} \Delta T, \quad (5)$$

$$\Delta T_{\text{me}} = \frac{C_{\text{te}}}{C_{\text{te}} + C_{\text{me}}} \Delta T = \frac{l_{\text{me}}\lambda_{\text{te}}}{l_{\text{me}}\lambda_{\text{te}} + l_{\text{te}}\lambda_{\text{me}}} \Delta T. \quad (6)$$

Unlike the previous case, the measured thermovoltage now has contributions from both the thermoelectric and the metal and is given by

$$U = S_{\text{te}}\Delta T_{\text{te}} + S_{\text{me}}\Delta T_{\text{me}} = \frac{S_{\text{te}}l_{\text{te}}\lambda_{\text{me}} + S_{\text{me}}l_{\text{me}}\lambda_{\text{te}}}{l_{\text{me}}\lambda_{\text{te}} + l_{\text{te}}\lambda_{\text{me}}} \Delta T. \quad (7)$$

This leads to

$$S = \frac{S_{\text{te}}l_{\text{te}}\lambda_{\text{me}} + S_{\text{me}}l_{\text{me}}\lambda_{\text{te}}}{l_{\text{me}}\lambda_{\text{te}} + l_{\text{te}}\lambda_{\text{me}}}. \quad (8)$$

The total Seebeck coefficient can be written using a material-related quantity, ε_λ, following the notation of our previous work about the thermoelectric properties of a film-substrate setup [42]:

$$S = \frac{S_{\text{te}} + \varepsilon_\lambda S_{\text{me}}}{1 + \varepsilon_\lambda} \quad \text{with } \varepsilon_\lambda = \frac{C_{\text{te}}}{C_{\text{me}}} = \frac{l_{\text{me}}\lambda_{\text{te}}}{l_{\text{te}}\lambda_{\text{me}}}. \quad (9)$$

Depending on the ratio between the individual thermal conductances, the total Seebeck coefficient lies between those of the thermoelectric material and the metal.

The finite resistivity further leads to a contribution of the metal to the total electrical resistance,

$$R = R_{\text{te}} + R_{\text{me}} = \rho_{\text{te}}\frac{l_{\text{te}}}{A} + \rho_{\text{me}}\frac{l_{\text{me}}}{A}, \quad (10)$$

and thus the electrical resistivity becomes

$$\rho = R\frac{A}{l} = \rho_{\text{te}}\left(\delta_{\text{te}} + \frac{\rho_{\text{me}}}{\rho_{\text{te}}}(1 - \delta_{\text{te}})\right), \quad (11)$$

which is a linear function depending on the volume fraction of the thermoelectric material. By introducing another quantity,

$$\varepsilon_\sigma = \frac{R_{\text{me}}}{R_{\text{te}}} = \frac{l_{\text{me}}\rho_{\text{me}}}{l_{\text{te}}\rho_{\text{te}}}, \quad (12)$$

Eq. (11) can be further simplified to

$$\rho = \rho_{\text{te}}\delta_{\text{te}}(1 + \varepsilon_\sigma). \quad (13)$$

Combining Eqs. (9) and (11) leads to the total power factor of the system:

$$\mathcal{P} = \frac{S^2}{\rho} = \left(\frac{S_{\text{te}} + \varepsilon_\lambda S_{\text{me}}}{1 + \varepsilon_\lambda}\right)^2 \frac{1}{\rho_{\text{te}}\delta_{\text{te}}(1 + \varepsilon_\sigma)}. \quad (14)$$

The different δ_{te} dependences of the Seebeck coefficient and electrical resistivity allows for extreme values of the

power factor if a well-conducting metal is incorporated into the thermoelectric material. The total power factor can also be written in terms of the individual power factors and the volume fraction of the thermoelectric material:

$$\mathcal{P}(\delta_{\text{te}}) = \frac{\left(\sqrt{\mathcal{P}_{\text{te}}} + \varepsilon_\lambda(\delta_{\text{te}})\sqrt{\rho_{\text{me}}/\rho_{\text{te}}}\,\text{sgn}(S_{\text{me}}/S_{\text{te}})\sqrt{\mathcal{P}_{\text{me}}}\right)^2}{\delta_{\text{te}}(1 + \varepsilon_\lambda(\delta_{\text{te}}))^2(1 + \varepsilon_\sigma(\delta_{\text{te}}))} \quad (15)$$

with the δ_{te}-dependent notation of the material-related quantities

$$\varepsilon_\varphi(\delta_{\text{te}}) = \frac{\varphi_{\text{te}}}{\varphi_{\text{me}}}\left(\frac{1}{\delta_{\text{te}}} - 1\right)\bigg|_{\varphi = \lambda, \sigma}. \quad (16)$$

A comparison between Eq. (15) and the results of Bergman and Fel can be observed in Appendix A for three selected systems calculated by the authors. The remarkable agreement between the models validates our assumptions and underscores the significance of the results presented here.

Within the above framework, the presence of a local maximum in PF depends on whether the decrease in thermovoltage caused by the metal is overcompensated by the increase in electrical conductivity. The consequences and relevance of the resulting PF enhancement will be discussed later. A comparison between the prediction of Eq. (15) and a $\text{Fe}_2\text{VAl}_{1.5}$-Cu composite is presented in Appendix B.

B. Figure of merit

Next, we will calculate the figure of merit zT of a binary composite, starting from an ideal metal with infinite conductivities. The total thermal conductance C can be calculated, in accordance with the electrical conductance, as

$$\frac{1}{C} = \frac{1}{C_{\text{te}}} = \frac{l_{\text{te}}}{\lambda_{\text{te}}A} := \frac{l_{\text{te}} + l_{\text{me}}}{\lambda A} \quad (17)$$

and thus

$$\lambda = \lambda_{\text{te}}\frac{1}{\delta_{\text{te}}}. \quad (18)$$

The thermal conductivity increases with decreasing volume fraction of the thermoelectric material, similar to the electrical conductivity [see Eq. (3)]. Combining Eq. (18) and Eq. (4) yields the total figure of merit

$$zT = \frac{\mathcal{P}}{\lambda}T = \frac{\mathcal{P}_{\text{te}}}{\lambda_{\text{te}}}T = zT_{\text{te}}. \quad (19)$$

The total thermal conductivity is modified when the thermal conductivity of the metal is no longer infinite. It then

becomes

$$\frac{1}{C} = \frac{1}{C_{\text{te}}} + \frac{1}{C_{\text{me}}} = \frac{l_{\text{te}}}{\lambda_{\text{te}}A} + \frac{l_{\text{me}}}{\lambda_{\text{me}}A} = \frac{l_{\text{te}} + l_{\text{me}}}{\lambda A}, \quad (20)$$

$$\lambda = \frac{\lambda_{\text{te}}}{\delta_{\text{te}}(1 + \varepsilon_\lambda)}. \quad (21)$$

From that, a convenient relation for the total figure of merit can be derived:

$$zT = \frac{\mathcal{P}}{\lambda}T = \frac{\left(\sqrt{zT_{\text{te}}} + \sqrt{\varepsilon_\lambda \varepsilon_\sigma}\, \text{sgn}(S_{\text{me}}/S_{\text{te}})\sqrt{zT_{\text{me}}}\right)^2}{(1 + \varepsilon_\lambda)(1 + \varepsilon_\sigma)}. \quad (22)$$

As an example, we calculated the thermoelectric power factor $\mathcal{P}$ and figure of merit zT of a composite consisting of Na-doped polycrystalline Sn-Se [10] as a high-performance thermoelectric material mixed with elemental Ag as well as another thermoelectric material, Se-doped Pb-Te [4] (see Fig. 2). While $\mathcal{P}$ reaches $\approx 250\mathcal{P}_{\text{te}}$ in Ag with 0.1% Sn-Se, the figure of merit in composites differs from the power factor in that a local maximum is absent. Hence, the zT of the composite always ranges between the values obtained for the pristine material, i.e., it is always smaller than the zT of the thermoelectric. A striking feature in Fig. 2 is that, in the case of a thermoelectric-metal composite, the figure of merit remains nearly constant even at very low volume fractions of the thermoelectric material due to the exceptionally large difference in the electrical and thermal conductivities of the two materials. This
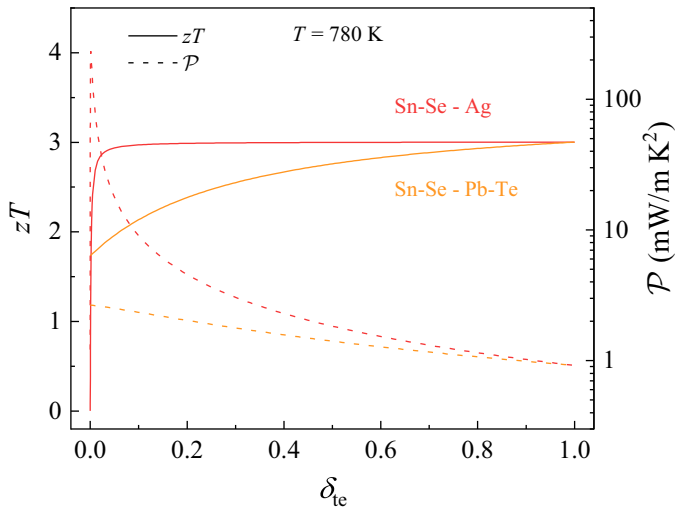

FIG. 2. Total figure of merit zT (solid lines) and power factor $\mathcal{P}$ (dashed lines) of a serial connection of Na-doped polycrystalline Sn-Se and Ag (red) and Se-doped Pb-Te (orange) at 780 K as functions of the volume fraction δ_{te} of Sn-Se, calculated from Eqs. (15) and (22). The values of the material properties were taken from the literature [4,10,43–45].

can be explained by the fact that in a serial configuration most of the temperature difference occurs across the thermoelectric material, preserving the thermovoltage, while the balance between increased electrical and thermal conductivity maintains zT. Deviation from ideal conduction in the metal is the only factor that decreases the overall zT [see Eq. (19)]. In contrast to that, both $\mathcal{P}$ and zT of a thermoelectric-thermoelectric composite show a more linear behavior as a function of the volume fraction, revealing the limitation of such systems and the necessity for additional effects that truly change the microscopic properties, such as interface scattering or diffusion.

The derivations of the thermoelectric properties presented here neglect interfaces between the constituents of the composite. Interfaces can lead to scattering of charge carriers and phonons and cause a modification of all thermoelectric quantities. Their influence is proportional to the electrical and thermal resistance as well as the number of interfaces. In Appendix C, a qualitative description of the effect of interfaces is provided. Nevertheless, the statements concluded from the ideal system are still valid if interface scattering is not the dominant mechanism determining the composite's performance.

III. CLEARING UP THE DELUSION: MICROSCOPIC VERSUS MACROSCOPIC PERFORMANCE

We point out that resistivity, thermal conductivity, and other quantities are material-specific intrinsic properties. In an electrical circuit consisting of several components with different properties—like the composites discussed here—the microscopic definition of the resistivity becomes ill-defined due to spatial inhomogeneity. Likewise, the PF becomes meaningless, as it does not reflect the total power output any more, as shown below. Instead, the proper quantities to compare the performance of such networks are total power output, heat conductance, and resistance. Such macroscopic quantities are generally more robust and less prone to mistakes and misinterpretations since they are measured directly and do not require considerations about the dimensions and microstructure of the system.

To further elucidate the meaning of the power factor of composites, we will compare $\mathcal{P}$, zT, and the power output for the three different systems comprising the state-of-the-art thermoelectric material Sn-Se and elemental Ag, as depicted in Fig. 3(a). These include a pure thermoelectric (I), a thermoelectric-metal composite (II), as well as the pure thermoelectric with reduced length (III). Again, interfaces will be neglected, which will yield different results than would be obtained experimentally. However, the informative value of the distinct difference between the setups is still assured.

It is well known that the maximum power transfer to a load connected to a thermoelectric generator occurs for
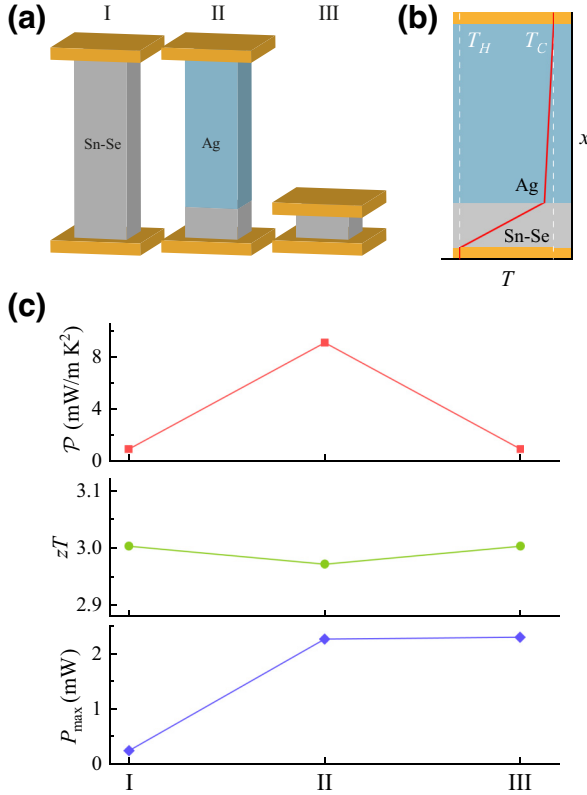
FIG. 3. (a) Sketch of the three systems compared in the text with respect to their thermoelectric performance: I, (Na-doped polycrystalline) Sn-Se; II, Sn-Se-Ag composite with $\delta_{te} = 0.1$; and III, Sn-Se with reduced length similar to system II. (b) Temperature profile of system II. (c) Power factor, figure of merit, and maximum power output for all three systems. The power output was calculated using $l = 1$ cm, $A = 1$ mm^2, $T = 300$ K, and $\Delta T = 100$ K. For the sake of simplicity, all thermoelectric properties were taken at 780 K [10,43–45].

equal resistances [46], thus

$$P_{\max} = \frac{U^2}{4R}, \tag{23}$$

with U and R being the total generated thermovoltage and resistance of the composite, respectively. Utilizing the definitions $U = S\Delta T$, $\mathcal{P} = S^2\sigma$, and $R = l/(\sigma A)$, which equates to a transformation of the composite into a single "average" material, Eq. (23) can be rewritten as

$$P_{\max} = \frac{A}{4l}\mathcal{P}^2\Delta T. \tag{24}$$

In Fig. 3(b), the temperature profile of system II is sketched. Unlike in systems I and III, where the temperature decreases linearly between the electrodes, the temperature drops mainly along the thermoelectric component

[compare Eqs. (5) and (6)]. The total power factor, figure of merit, and power output are shown in Fig. 3(c).

At first glance, the Sn-Se-Ag composite (II) seems to perform better than pure Sn-Se (I) in terms of power factor and power output, while reducing the figure of merit only moderately. Incorporating metal components into the thermoelectric material improves the power generated by reducing the total resistivity while the Seebeck coefficient S remains almost unaffected, thereby seemingly decoupling S and σ, two transport properties that are usually difficult to enhance simultaneously [47]. However, it is not the metal *per se* that improves the performance but rather the length reduction of the thermoelectric, while the temperature drop across the thermoelectric remains the same—an approximation that cannot always be realized in applications.

Indeed, a comparison between systems II and III shows that, for the same volume of the active thermoelectric component, the power output is marginally higher without the metal despite the fact that the metal composite has a 10 times higher power factor. Thus, the enhancement of the power factor found by several studies and also in the present work merely results from a nonsensical comparison of two materials with different volume fractions of the active thermoelectric component. Therefore, the power factor is no longer a valid indicator for thermoelectric performance in composite materials. Since a large $\mathcal{P}$ indicates neither a higher zT nor a higher power output in such composites, the power factor becomes a meaningless parameter for evaluating composite materials or devices. Only in fixed-length setups, if power output is more critical than efficiency, can the use of composites significantly increase power output by reducing the volume fraction of the thermoelectric material and lowering the resistance—given that the same temperature drop can be realized across the thermoelectric material with reduced length, i.e., a significantly enhanced temperature gradient dT/dl.

The showcase presented above nicely illustrates the necessity to consider the dimensions of the material if inhomogeneities are present, as is the case in composites. Accordingly, the use of macroscopic quantities is inevitable.

Another potential application for thermoelectric materials with high power factors is the so-called active cooling, which combines traditional heat conduction with the Peltier effect to enhance cooling capabilities [48]. In this context, a large thermal conductivity and power factor are desired to maximize the effective thermal conductivity λ_{eff}:

$$\lambda_{\text{eff}} = \left(\lambda + \frac{\mathcal{P}T_H^2}{2\Delta T}\right), \tag{25}$$

with the temperature of the hot side T_H. Active cooling does indeed look like a promising application when

composites are compared to conventional materials (see Appendix D).

However, it is important to examine the macroscopic quantity—the actual cooling power—as the high power factor can be misleading and give a false impression of the performance. A closer look at the cooling power,

$$\frac{dQ}{dt} = \lambda_{\text{eff}} \frac{A}{l} \Delta T = \left(C + \frac{S^2 T_H^2}{2R\Delta T} \right) \Delta T, \quad (26)$$

expressed with the macroscopic quantities $C = \lambda(A/l)$ and $S^2/R = \mathcal{P}(A/l)$, reveals the inferiority of composites to pure thermoelectrics. While the resistance can be decreased by substituting part of the thermoelectric material with a metal, thus enhancing the cooling power, the performance is always worse compared to the pure thermoelectric with reduced length. Similar to Eq. (24), the metal-incorporated material appears better due to a comparison of different amounts of thermoelectric material.

IV. THE BEST COMPOSITE

Before exploring the potential applications of composites, it is important to acknowledge that the formulas used to predict the thermoelectric performance are subject to ideal conditions and may not accurately reflect real-world scenarios. This is because they do not account for the impact of external factors such as contact resistances and inter-phase scattering. As a result, the actual performance may differ from predicted values. That being said, realistic composites with arbitrarily arranged microstructure can be approximated by a model where one component adopts a spherical shape enclosed by the other, which shows the same thermoelectric tendency as the parallel slab model [31]. Thus, the following statements should be valid in most cases.

As we have shown in this work, an enhancement of the thermoelectric properties due to a combination of a high-performance thermoelectric and a simple metal in a serial configuration is not possible without intrinsic property changes of the individual materials comprising the composite, such as interface effects. When considering the significant impact of these secondary effects on the properties of real composite materials, and the frequent use of composites to improve the figure of merit, it prompts the question of which materials are best suited for making composites.

As can be seen in Fig. 2, the total figure of merit zT stays almost constant down to a few percent of the volume fraction of the thermoelectric material when a well-conducting metal is used as the second material. This opens a gigantic playground to reduce the lattice thermal conductivity of the thermoelectric material via increased boundary scattering, as sketched in Fig. 4. Although the reduction of the thermal conductivity is shown for an oversimplified δ_{te} relation, it
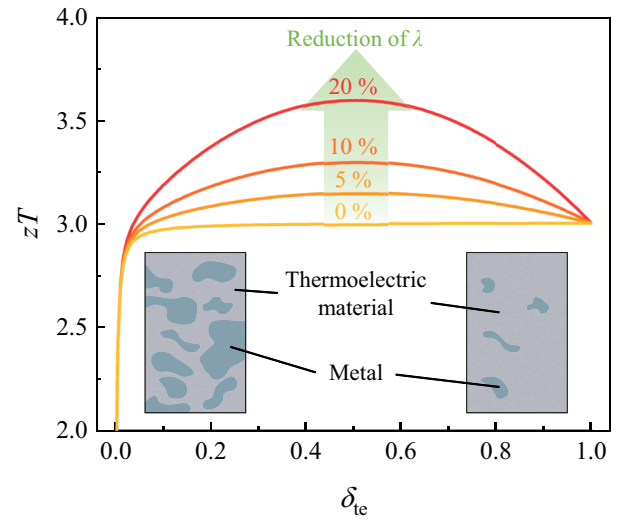

FIG. 4. Figure of merit zT of a Sn-Se-Ag composite for different reductions of lambda due to increased scattering on the metallic structures. The reduction was calculated from a simple δ_{te}-dependent relation, $\lambda_{\text{red}} = \lambda/[1 + a\delta_{\text{te}}(1 - \delta_{\text{te}})]$, with a chosen such that the reduction equals 5%, 10%, and 20% for $\delta_{\text{te}} = 0.5$.

is clearly visible that scattering of phonons with long mean free paths on mesoscale-sized metallic structures will have a positive effect on the performance [23]. Hence, adding a nonsoluble and highly conducting metal is a cheap and profitable strategy to achieve a larger figure of merit or reduce the amount of the thermoelectric material.

V. CONCLUSION

We recalculated the results of Bergman and Fel [31] from a simple model while avoiding any approximations. In alignment with their model, we neglected boundary effects, such as interface electrical and thermal resistances. Despite this indisputable simple view on the matter, our results shed new light on the origin of the extreme values of power factor derived for composites, which are caused by a drastic reduction of the resistance while the thermovoltage only changes moderately due to the nonuniform temperature gradient. We further elucidated the misleading meaning of the power factor by comparing measurable macroscopic quantities such as the power output to pure thermoelectric materials. We strongly advise using the robust and error-resistant figure of merit zT when comparing the performance of composites; similar to electrical resistivity and thermal conductivity, the power factor remains a well-defined quantity only for microscopically homogeneous systems. Lastly, we showed that, in theory, the best thermoelectric composite consists of a high-zT thermoelectric and a simple metal with maximal thermal and electrical conductivity.

APPENDIX A: COMPARISON WITH THE BERGMAN MODEL

Figure 5 compares our model with the results of Bergman and Fel [31]. The models show excellent agreement despite the different mathematical approaches. As discussed in the main text, the total power factor shows a local maximum if the incorporation of a metal into the main phase decreases the resistivity faster than the square of the Seebeck coefficient. Here, this is only the case in $(Bi_2Te_3)_{0.2}(Sb_2Te_3)_{0.8}$-Al, where a sufficient ratio of the electrical conductivities ($\sigma_{me}/\sigma_{te} = 270$) and thermal conductivities ($\lambda_{me}/\lambda_{te} = 67.2$) is given. In $CoSb_3$-Ni, the thermal conductivities are too similar ($\lambda_{me}/\lambda_{te} = 1.8$), which causes a significant temperature drop inside the Ni phase and makes an enhancement impossible. The Bi_2Te_3-Pb-Te composite instructively shows that a combination of two thermoelectrics only worsens the overall performance if not for additional scattering, diffusion, or other interrelated effects. The extremely low power factor in $CoSb_3$-Ni for $\delta_{te} \approx 0.08$ is due to the opposite signs of the Seebeck coefficients, which leads to a cancelation of the opposing thermovoltages.

APPENDIX B: EXPERIMENTAL VALIDATION

To validate the results from our model, we compared the experimental power factor of a serial $Fe_2VAl_{1.5}$-Cu composite with the predicted values in Fig. 6. The power factor reaches 4.5 mW/me K^2 at 350 K for a volume fraction of $Fe_2VAl_{1.5}$ of $\delta_{te} = 0.25 \pm 0.1$, a value that is more than four times larger than that of the pristine thermoelectric. The composite was made using spark plasma sintering with a pressure of 50 MPa and a temperature of 1100 °C.

APPENDIX C: CONSIDERATION OF SMALL INTERFACE RESISTANCES

In a composite, the interactions at the interfaces between different constituents can alter its thermoelectric performance. These interfaces can cause scattering of charge carriers, resulting in locally reduced electrical and thermal conductivities. More importantly, phonon scattering on interface structures hampers heat conduction, lowering the overall thermal conductivity but also causing a discontinuity of the temperature at the interface. Such a scenario is illustrated in Fig. 7. Similar to the derivation in the main text, the temperature drop across both the thermoelectric material and the metal can be derived:

$$\Delta T_{te} = \frac{C_{int}C_{me}}{C_{int}C_{te} + C_{int}C_{me} + C_{te}C_{me}}\Delta T, \quad (C1)$$

FIG. 6. Comparison of the power factor of a $Fe_2VAl_{1.5}$-Cu composite and the values predicted by the model presented in the main text. The composite was measured for 25%, 70%, and 100% volume fraction of the thermoelectric material. Because of the irregular interface and uncertainty in the determination of the volume fraction due to the finite thickness of the thermocouple, an error of $\pm 10\%$ was assumed for the volume fraction. The inset shows the experimental setup for the measurement of the system with $\delta_{te} = 0.7$. The thermoelectric properties of $Fe_2VAl_{1.5}$ and Cu were taken from Ref. [49] and Refs. [43,44], respectively.
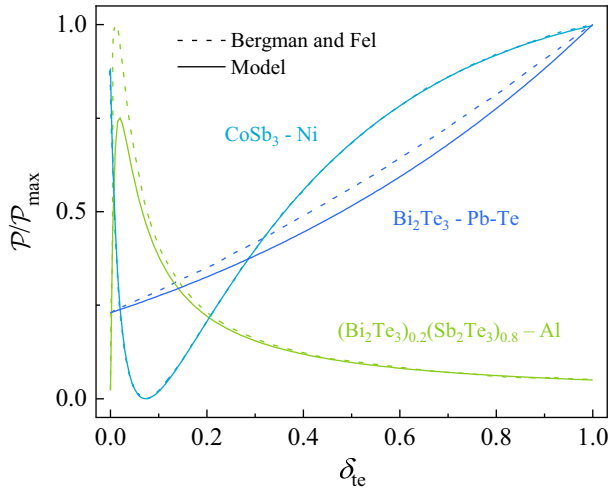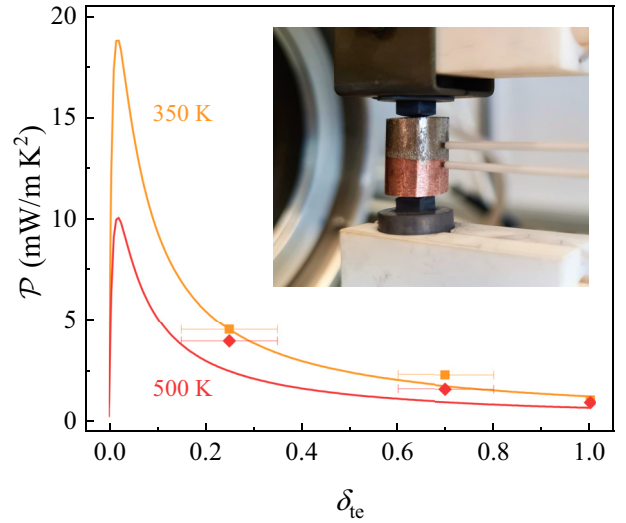

FIG. 5. Comparison of the total power factor $\mathcal{P}$ between the model of Bergman and Fel [31] and our model, applied on three different systems. The reference line of the $CoSb_3$-Ni system is not visible due to its excellent alignment with our model. The values of the individual thermoelectric properties were taken from Ref. [31].
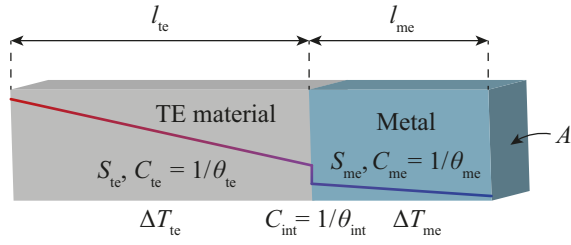
FIG. 7. Schematic of a serial connection of a thermoelectric material (length l_{te}) and a metal (length l_{me}), incorporating an interface thermal resistance. Both materials possess individual Seebeck coefficients S and thermal conductances $C = 1/\theta$, while the interface is characterized by an additional thermal conductance. The temperature differences across the thermoelectric material and the metal are denoted as ΔT_{te} and ΔT_{me}, respectively. The solid line sketches the temperature profile.

$$\Delta T_{me} = \frac{C_{int}C_{te}}{C_{int}C_{te} + C_{int}C_{me} + C_{te}C_{me}}\Delta T, \quad (C2)$$

with the thermal conductances $C_j = \lambda_j A/l_j$ and $j = \{te, me, int\}$ denoting the thermoelectric, metal, and interface, respectively.

Using the thermal resistance $\theta_j = 1/C_j$, these equations can be written more conveniently as

$$\Delta T_{te} = \frac{\theta_{te}}{\theta_{te} + \theta_{me} + \theta_{int}}\Delta T = \left(1 + \frac{\theta_{int}}{\theta_{te} + \theta_{me}}\right)^{-1}\Delta T_{te}^{id} \quad (C3)$$

and

$$\Delta T_{me} = \left(1 + \frac{\theta_{int}}{\theta_{te} + \theta_{me}}\right)^{-1}\Delta T_{me}^{id}. \quad (C4)$$

Here, ΔT_{te}^{id} and ΔT_{me}^{id} represent the temperature drops in the ideal system without interface resistances.

The measured thermopower is given by

$$U = S_{te}\Delta T_{te} + S_{me}\Delta T_{me} = \left(1 + \frac{\theta_{int}}{\theta_{te} + \theta_{me}}\right)^{-1}U^{id}. \quad (C5)$$

As expected, the measured voltage is smaller than that of the ideal system U^{id} without an interface. For a larger number N of interfaces, the Seebeck coefficient can be written as

$$S = \left(1 + \frac{N\theta_{int}}{\theta_{te} + \theta_{me}}\right)^{-1}S^{id}. \quad (C6)$$

Furthermore, an equivalent trend can be observed for the overall thermal conductivity of the system. Taking

into account the influence of the interface, the thermal resistance becomes

$$\theta = \theta_{te} + \theta_{me} + N\theta_{int} = \theta_{te}\left(1 + \varepsilon_\lambda + \frac{N\theta_{int}}{\theta_{te}}\right). \quad (C7)$$

This leads to the following expression for the thermal conductivity:

$$\lambda = \frac{\lambda_{te}}{\delta_{te}(1 + \varepsilon_\lambda + N\theta_{int}/\theta_{te})} = \left(1 + \frac{N\theta_{int}}{\theta_{te} + \theta_{me}}\right)^{-1}\lambda^{id}. \quad (C8)$$
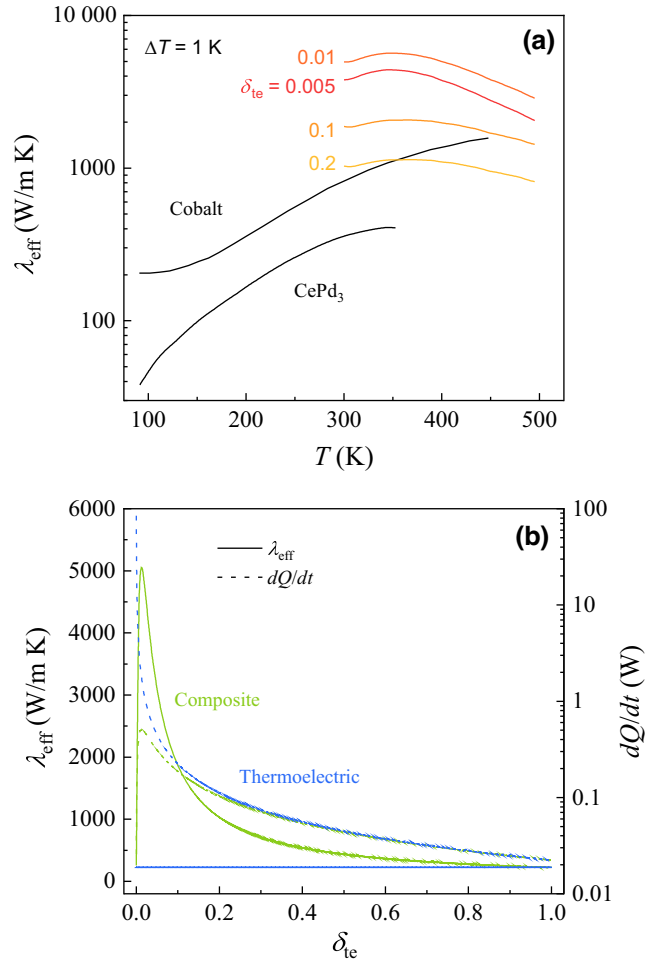

FIG. 8. (a) Effective thermal conductivity as a function of the temperature T for Bi_2Te_3-Al composites with different volume fractions of the thermoelectric δ_{te}, calculated from the formula shown in the main text. The black solid lines show reference materials [48]. (b) Volume-fraction-dependent effective thermal conductivity (solid lines) and cooling power (dashed lines) of a composite and a single thermoelectric material with length equal to the share in the composite. The properties of Bi_2Te_3 and Al were taken from the literature [2,43,44,50].

A similar impact of the interface can be found for the electrical resistivity:

$$\rho = \left(1 + \frac{N\rho_{\text{int}}}{\rho_{\text{te}} + \rho_{\text{me}}}\right)\rho^{\text{id}}, \tag{C9}$$

with ρ_{int} being the electrical resistance of the interface.

In summary, the interfaces between the constituents of a composite can influence all thermoelectric properties, namely causing a reduction of the Seebeck coefficient as well as the electrical and thermal conductivities. The extent of this influence depends on the electrical and thermal resistances of the interface compared to the values of the constituents, as well as the number of interfaces, reflecting the structure of the composite.

APPENDIX D: ACTIVE COOLING

Figure 8(a) shows the effective thermal conductivity λ_{eff} of a Bi_2Te_3-Al composite for different volume fractions of the thermoelectric and compares it with cobalt and $CePd_3$ [48]. It shows that λ_{eff} is significantly enhanced in metal-dominated composites. This might cause a false interpretation of measurement results. A comparison of the macroscopic quantity, the cooling power dQ/dt, reveals the inferiority of composites compared to single-phase materials [see Fig. 8(b)]. For all volume fractions, the composite has a lower cooling efficiency despite the higher effective thermal conductivity. This shows, similar to the thermoelectric efficiency described in the main text, that a comparison of the macroscopic quantities is necessary to obtain an unbiased insight on a material's quality.

[1] L. Yang, Z.-G. Chen, M. Hong, G. Han, and J. Zou, Enhanced thermoelectric performance of nanostructured Bi_2Te_3 through significant phonon scattering, ACS Appl. Mater. Interfaces **7**, 23694 (2015).

[2] I. T. Witting, T. C. Chasapis, F. Ricci, M. Peters, N. A. Heinz, G. Hautier, and G. J. Snyder, The thermoelectric properties of bismuth telluride, Adv. Electron. Mater. **5**, 1800904 (2019).

[3] J. P. Heremans, V. Jovovic, E. S. Toberer, A. Saramat, K. Kurosaki, A. Charoenphakdee, S. Yamanaka, and G. J. Snyder, Enhancement of thermoelectric efficiency in PbTe by distortion of the electronic density of states, Science **321**, 554 (2008).

[4] Y. Pei, X. Shi, A. LaLonde, H. Wang, L. Chen, and G. J. Snyder, Convergence of electronic bands for high performance bulk thermoelectrics, Nature **473**, 66 (2011).

[5] Y. Pei, A. LaLonde, S. Iwanaga, and G. J. Snyder, High thermoelectric figure of merit in heavy hole dominated PbTe, Energy Environ. Sci. **4**, 2085 (2011).

[6] G. Joshi, H. Lee, Y. Lan, X. Wang, G. Zhu, D. Wang, R. W. Gould, D. C. Cuff, M. Y. Tang, and M. S. Dresselhaus,

et al., Enhanced thermoelectric figure-of-merit in nanostructured p-type silicon germanium bulk alloys, Nano Lett. **8**, 4670 (2008).

[7] X. Wang, H. Lee, Y. Lan, G. Zhu, G. Joshi, D. Wang, J. Yang, A. Muto, M. Tang, and J. Klatsky, et al., Enhanced thermoelectric figure of merit in nanostructured n-type silicon germanium bulk alloy, Appl. Phys. Lett. **93**, 193121 (2008).

[8] L.-D. Zhao, S.-H. Lo, Y. Zhang, H. Sun, G. Tan, C. Uher, C. Wolverton, V. P. Dravid, and M. G. Kanatzidis, Ultralow thermal conductivity and high thermoelectric figure of merit in SnSe crystals, Nature **508**, 373 (2014).

[9] L.-D. Zhao, C. Chang, G. Tan, and M. G. Kanatzidis, SnSe: A remarkable new thermoelectric material, Energy Environ. Sci. **9**, 3044 (2016).

[10] C. Zhou, Y. K. Lee, Y. Yu, S. Byun, Z.-Z. Luo, H. Lee, B. Ge, Y.-L. Lee, X. Chen, and J. Y. Lee, et al., Polycrystalline SnSe with a thermoelectric figure of merit greater than the single crystal, Nat. Mater. **20**, 1378 (2021).

[11] C. Uher, in *Semiconductors and semimetals*, Vol. 69 (Elsevier, 2001), p. 139.

[12] X. Shi, J. Yang, J. R. Salvador, M. Chi, J. Y. Cho, H. Wang, S. Bai, J. Yang, W. Zhang, and L. Chen, Multiple-filled skutterudites: High thermoelectric figure of merit through separately optimizing electrical and thermal transports, J. Am. Chem. Soc. **133**, 7837 (2011).

[13] G. Rogl, A. Grytsiv, K. Yubuta, S. Puchegger, E. Bauer, C. Raju, R. Mallik, and P. Rogl, In-doped multifilled n-type skutterudites with $ZT = 1.8$, Acta Mater. **95**, 201 (2015).

[14] C. Fu, T. Zhu, Y. Liu, H. Xie, and X. Zhao, Band engineering of high performance p-type FeNbSb based half-Heusler thermoelectric materials for figure of merit $zT > 1$, Energy Environ. Sci. **8**, 216 (2015).

[15] C. Fu, S. Bai, Y. Liu, Y. Tang, L. Chen, X. Zhao, and T. Zhu, Realizing high figure of merit in heavy-band p-type half-Heusler thermoelectric materials, Nat. Commun. **6**, 8144 (2015).

[16] W. G. Zeier, J. Schmitt, G. Hautier, U. Aydemir, Z. M. Gibbs, C. Felser, and G. J. Snyder, Engineering half-Heusler thermoelectric materials using Zintl chemistry, Nat. Rev. Mater. **1**, 1 (2016).

[17] A. L. Prieto, M. S. Sander, M. S. Martin-Gonzalez, R. Gronsky, T. Sands, and A. M. Stacy, Electrodeposition of ordered Bi_2Te_3 nanowire arrays, J. Am. Chem. Soc. **123**, 7160 (2001).

[18] O. Rabina, Y.-M. Lin, and M. S. Dresselhaus, Anomalously high thermoelectric figure of merit in $Bi_{1-x}Sb_x$ nanowires by carrier pocket alignment, Appl. Phys. Lett. **79**, 81 (2001).

[19] R. Venkatasubramanian, E. Siivola, T. Colpitts, and B. O'quinn, Thin-film thermoelectric devices with high room-temperature figures of merit, Nature **413**, 597 (2001).

[20] B. Hinterleitner, I. Knapp, M. Poneder, Y. Shi, H. Müller, G. Eguchi, C. Eisenmenger-Sittner, M. Stöger-Pollach, Y. Kakefuda, and N. Kawamoto, et al., Thermoelectric performance of a metastable thin-film Heusler alloy, Nature **576**, 85 (2019).

[21] W. Kim, J. Zide, A. Gossard, D. Klenov, S. Stemmer, A. Shakouri, and A. Majumdar, Thermal Conductivity Reduction and Thermoelectric Figure of Merit Increase by

Embedding Nanoparticles in Crystalline Semiconductors, Phys. Rev. Lett. **96,** 045901 (2006).

[22] Z. Xiong, X. Chen, X. Zhao, S. Bai, X. Huang, and L. Chen, Effects of nano-TiO_2 dispersion on the thermoelectric properties of filled-skutterudite $Ba_{0.22}Co_4Sb_{12}$, Solid State Sci. **11,** 1612 (2009).

[23] K. Biswas, J. He, I. D. Blum, C.-I. Wu, T. P. Hogan, D. N. Seidman, V. P. Dravid, and M. G. Kanatzidis, High-performance bulk thermoelectrics with all-scale hierarchical architectures, Nature **489,** 414 (2012).

[24] F. Delorme, P. Diaz-Chao, E. Guilmeau, and F. Giovannelli, Thermoelectric properties of $Ca_3Co_4O_9$-Co_3O_4 composites, Ceram. Int. **41,** 10038 (2015).

[25] J. Zhang, H. Ming, D. Li, X. Qin, J. Zhang, L. Huang, C. Song, and L. Wang, Ultralow thermal conductivity and high thermoelectric performance of n-type $Bi_2Te_{2.7}Se_{0.3}$-based composites incorporated with GaAs nanoinclusions, ACS Appl. Mater. Interfaces **12,** 37155 (2020).

[26] N. Neophytou, X. Zianni, H. Kosina, S. Frabboni, B. Lorenzi, and D. Narducci, Simultaneous increase in electrical conductivity and Seebeck coefficient in highly boron-doped nanocrystalline Si, Nanotechnology **24,** 205402 (2013).

[27] B. Nan, X. Song, C. Chang, K. Xiao, Y. Zhang, L. Yang, S. Horta, J. Li, K. H. Lim, and M. Ibáñez, *et al.*, Bottom-up synthesis of SnTe-based thermoelectric composites, ACS Appl. Mater. Interfaces **15,** 23380 (2023).

[28] X. Yang, X. Qin, J. Zhang, D. Li, H. Xin, and M. Liu, Enhanced thermopower and energy filtering effect from synergetic scattering at heterojunction potentials in the thermoelectric composites with semiconducting nanoinclusions, J. Alloys. Compd. **558,** 203 (2013).

[29] B. Madavali, H.-S. Kim, K.-H. Lee, and S.-J. Hong, Enhanced Seebeck coefficient by energy filtering in Bi-Sb-Te based composites with dispersed Y_2O_3 nanoparticles, Intermetallics **82,** 68 (2017).

[30] N. Neophytou, S. Foster, V. Vargiamidis, G. Pennelli, and D. Narducci, Nanostructured potential well/barrier engineering for realizing unprecedentedly large thermoelectric power factors, Mater. Today Phys. **11,** 100159 (2019).

[31] D. J. Bergman and L. G. Fel, Enhancement of thermoelectric power factor in composite thermoelectrics, J. Appl. Phys. **85,** 8205 (1999).

[32] D. J. Bergman and O. Levy, Thermoelectric properties of a composite medium, J. Appl. Phys. **70,** 6821 (1991).

[33] H. Odahara, O. Yamashita, K. Satou, S. Tomiyoshi, J.-i. Tani, and H. Kido, Increase of the thermoelectric power factor in Cu/Bi/Cu, Ni/Bi/Ni, and Cu/Bi/Ni composite materials, J. Appl. Phys. **97,** 103722 (2005).

[34] O. Yamashita, H. Odahara, and K. Satou, Enhancement in thermoelectric power factor of M/T/N and M/Bi/M/Bi/M (M and N = Cu or Ni) composite devices welded with T = Bi or $Bi_{0.88}Sb_{0.12}$ alloy, J. Mater. Sci. **40,** 1071 (2005).

[35] M. Mikami, N. Ando, and R. Funahashi, The effect of Ag addition on electrical properties of the thermoelectric compound $Ca_3Co_4O_9$, J. Solid State Chem. **178,** 2186 (2005).

[36] O. Yamashita, H. Odahara, K. Satou, and S. Tomiyoshi, Enhancement of the thermoelectric power factor in Ag/Bi-Te/Ag composite devices, J. Mater. Sci. **41,** 3089 (2006).

[37] J. Heremans and C. Jaworski, Experimental study of the thermoelectric power factor enhancement in composites, Appl. Phys. Lett. **93,** 122107 (2008).

[38] A. Sotelo, M. Torres, G. Constantinescu, S. Rasekh, J. Diez, and M. Madre, Effect of Ag addition on the mechanical and thermoelectric performances of annealed $Bi_2Sr_2Co_{1.8}O_x$ textured ceramics, J. Eur. Ceram. Soc. **32,** 3745 (2012).

[39] F. Kahraman, M. Madre, S. Rasekh, C. Salvador, P. Bosque, M. Torres, J. Diez, and A. Sotelo, Enhancement of mechanical and thermoelectric properties of $Ca_3Co_4O_9$ by Ag addition, J. Eur. Ceram. Soc. **35,** 3835 (2015).

[40] B. Zhan, Y. Liu, J. Lan, C. Zeng, Y.-H. Lin, and C.-W. Nan, Enhanced thermoelectric performance of Bi_2O_2Se with Ag addition, Materials **8,** 1568 (2015).

[41] S. D. Sharma, B. Khasimsaheb, Y. Chen, and S. Neeleshwar, Enhanced thermoelectric performance of Cu_2ZnSnS_4 (CZTS) by incorporating Ag nanoparticles, Ceram. Int. **45,** 2060 (2019).

[42] A. Riss, M. Stöger, M. Parzer, F. Garmroudi, N. Reumann, B. Hinterleitner, T. Mori, and E. Bauer, Criteria for erroneous substrate contribution to the thermoelectric performance of thin films, Phys. Rev. Appl. **19,** 054024 (2023).

[43] C. Ho, M. Ackerman, K. Wu, S. Oh, and T. Havill, Thermal conductivity of ten selected binary alloy systems, J. Phys. Chem. Ref. Data **7,** 959 (1978).

[44] C. Y. Ho, M. Ackerman, K. Wu, T. Havill, R. Bogaard, R. Matula, S. Oh, and H. James, Electrical resistivity of ten selected binary alloy systems, J. Phys. Chem. Ref. Data **12,** 183 (1983).

[45] C. Ho, R. Bogaard, T. Chi, T. Havill, and H. James, Thermoelectric power of selected metals and binary alloy systems, Thermochim. Acta **218,** 29 (1993).

[46] J. Chen, Z. Yan, and L. Wu, The influence of Thomson effect on the maximum power output and maximum efficiency of a thermoelectric generator, J. Appl. Phys. **79,** 8823 (1996).

[47] G. J. Snyder and E. S. Toberer, Complex thermoelectric materials, Nat. Mater. **7,** 105 (2008).

[48] M. Adams, M. Verosky, M. Zebarjadi, and J. Heremans, Active Peltier coolers based on correlated and magnon-drag metals, Phys. Rev. Appl. **11,** 054008 (2019).

[49] M. Parzer, F. Garmroudi, A. Riss, S. Khmelevskyi, T. Mori, and E. Bauer, High solubility of Al and enhanced thermoelectric performance due to resonant states in Fe_2VAl_x, Appl. Phys. Lett. **120,** 071901 (2022).

[50] R. J. Gripshover, J. B. VanZytveld, and J. Bass, Thermopower of pure aluminum, Phys. Rev. **163,** 598 (1967).